Integrated Wind Turbine Selection and Layout Optimization for Coastal Vietnam Using Symbiotic Organisms Search

Khoa Dang Nguyen[1,2], Tinh Trung Tran[2], Tuan Hoang Minh Nguyen[1,3], Vu Anh Le[4], and Dieu Ngoc Vo[1,3*]

ARTICLE INFO

Article history:
Received: 2 October 2025
Revised: 16 December 2025
Accepted: 2 January 2026
Online: 20 July 2026

Keywords:
Annual energy production
Capacity factor
Coastal wind resource
Symbiotic Organisms Search
Wake modeling
Wind farm layout optimization

ABSTRACT

Maximizing wind farm performance requires a rigorous integration of turbine technology selection and layout optimization, particularly in coastal environments where wind variability and terrain-induced wake interactions can significantly undermine energy yield. This study introduces a unified and data-driven framework that combines wind-speed probability characterization, turbine power-curve matching, and an enhanced Symbiotic Organisms Search (SOS) algorithm to jointly optimize turbine choice and spatial configuration for a Vietnamese coastal wind farm. Three modern turbine models—3.0 MW, 3.45 MW, and 4.2 MW—are systematically evaluated to quantify how rated wind speed, rotor diameter, and aerodynamic behavior shape wake losses, capacity factor (CF), and annual energy production (AEP). Results demonstrate that the 3.0 MW turbine provides the most advantageous balance between aerodynamic compatibility, layout density, and wake performance, achieving superior AEP of 188.29 GWh/year, the highest capacity factor of 34.12%, and the lowest wake losses of 8.2% under the dominant wind regime of 7–11 m/s. The turbine's smaller rotor diameter (90 m) enables the deployment of 21 units—the highest density among the three options—while maintaining optimal inter-turbine spacing. The SOS algorithm exhibits exceptional optimization capability, outperforming PSO and GA in convergence speed, robustness, and solution quality, delivering 4.0–4.6% improvements in AEP over PSO and up to 2.2 GWh/year over GA. The proposed framework delivers a scalable and transferable methodology for medium-wind and coastal wind-farm development, offering actionable evidence to guide turbine procurement, spatial planning, and long-term energy investment strategies in emerging wind markets.

1. INTRODUCTION

Global commitments to achieve Net-Zero emissions accelerate the worldwide deployment of renewable energy systems [1], [2]. Among these systems, wind power is a central pillar of the energy transition due to continuous reductions in technology costs, significant improvements in turbine efficiency, and the suitability of modern turbines for large-scale onshore and coastal applications [3]–[5]. Vietnam possesses substantial wind potential driven by monsoonal circulation and extensive coastlines [6], [7].

Despite this potential, transforming Vietnam's wind resources into effective power generation remains challenging. The performance of a wind farm is highly sensitive to turbine placement, wake interactions, terrain characteristics, and especially the suitability of turbine capacity relative to site-specific wind conditions. Suboptimal layout configurations or inappropriate turbine ratings can intensify wake losses and lead to substantial reductions in annual energy production (AEP) and capacity factor (CF) [8], [9]. Additionally, monsoon-driven seasonal variability introduces further uncertainty that requires careful consideration in early-stage design [10], [11].

Designing an efficient wind farm therefore necessitates the simultaneous optimization of turbine positions and turbine capacity selection. However, the wind farm layout optimization (WFLO) problem is intrinsically nonlinear, discrete, and multimodal, resulting in an enormous combinatorial search space that renders classical optimization impractical. Traditional design practices—such as uniform spacing heuristics or expert judgement—often fail to account for complex aerodynamic interactions, heterogeneous terrain effects, and multi-directional wind

[1]*Faculty of Electrical and Electronic Engineering, Ho Chi Minh City University of Technology, 268 Ly Thuong Kiet Street, Dien Hong Ward, Ho Chi Minh City, Viet Nam.*
[2]*College of Engineering Technology, Can Tho University, Viet Nam.*
[3]*Vietnam National University Ho Chi Minh, Linh Xuan Ward, Ho Chi Minh City, Vietnam.*
[4]*Dong Nai Power Company, Southerm Power Coporation, Dong Nai Province, Vietnam.*
**Corresponding author:* Dieu Ngoc Vo; Email: vndieu@hcmut.edu.vn and Khoa Dang Nguyen; Email: nguyendangkhoa.sdh21@hcmut.edu.vn.

regimes, leading to conservative or suboptimal solutions [12]–[15].

Metaheuristic algorithms have been increasingly adopted to address such high-dimensional nonlinear problems due to their strong global search capabilities. Methods such as Symbiotic Organisms Search (SOS), Grasshopper Optimization Algorithm (GOA), and other swarm-based approaches have shown promising results in renewable energy and layout optimization domains [16]–[18]. However, several research gaps remain. First, many existing studies rely on simplified or synthetic wind datasets rather than long-term field measurements, limiting applicability in regions characterized by strong seasonal variability such as coastal Vietnam [19], [20]. Second, despite its significant influence on wake behavior and energy yield, turbine capacity selection is often treated as a secondary problem and rarely integrated as a core decision variable within WFLO [21], [22]. Third, comparative assessments of commercial turbine models within a unified optimization framework are limited, reducing the practical relevance of research outcomes for developers and policymakers [23].

This study addresses these critical gaps by introducing a novel integrated framework that fundamentally differs from prior WFLO research in four key aspects. First, unlike conventional sequential approaches where turbine selection precedes layout optimization, our framework treats both decisions as coupled optimization variables within a unified search process, explicitly capturing the interdependencies between turbine technical specifications (rotor diameter, rated power, power curve characteristics) and site-specific wake interaction patterns. Second, we employ one full year of high-resolution wind measurements (10-minute intervals) from a coastal Vietnamese site, incorporating realistic seasonal monsoon variability and multi-directional wind regimes that are absent in synthetic or short-term datasets commonly used in literature [12]–[15]. Third, our comparative assessment systematically evaluates three commercially available turbine models (3.0 MW, 3.45 MW, and 4.2 MW) across multiple performance dimensions—aerodynamic efficiency, wake behavior, spatial deployment constraints, and economic viability—within an identical optimization framework, providing actionable insights for project developers rather than theoretical algorithm comparisons. Fourth, by integrating detailed terrain characterization, site-specific Weibull distributions, and the Jensen-2D wake model with the SOS algorithm, we demonstrate that turbine capacity selection fundamentally alters optimal spatial configurations, and that joint optimization yields 4.0–4.6% higher annual energy production compared to sequential design approaches. These contributions advance WFLO methodology from theoretical algorithm development toward practical decision-support tools for emerging wind markets.

To address these gaps, this study proposes a comprehensive wind farm design framework based on the Symbiotic Organisms Search (SOS) algorithm, specifically tailored to coastal wind conditions in Vietnam. The framework integrates one year of high-resolution wind measurements, detailed terrain characterization, and three commercial turbine capacities (3.0 MW, 3.45 MW, and 4.2 MW) to jointly optimize turbine placement and turbine rating selection. By incorporating realistic wake modeling and site-specific wind distributions, the proposed approach enhances the accuracy of AEP estimation, improves turbine model selection, and supports the development of more efficient coastal wind farm layouts in emerging markets.

2. MATHEMATICAL MODEL

2.1 Key Assumptions

To develop a general model for the wind turbine layout optimization problem, particularly for existing wind farms requiring expansion or capacity enhancement, a set of assumptions is considered [24]. These assumptions can be easily modified to suit specific applications.

• **Assumption 1:** New turbines planned for installation are assumed identical in turbine characteristics and rated power

• **Assumption 2:** Number of turbines N is known and fixed

• **Assumption 3:** Wind farm is arranged in a (x, y) coordinate plane with turbine positions at (x_i, y_i, $i=1, ..., N$)

• **Assumption 4:** Wind speed v follows Weibull distribution for each wind direction θ [25]

• **Assumption 5:** For wind direction θ, all turbine rotors are perpendicular to the wind direction

2.2 Wake Effect Model

Wake effect is one of the most critical factors in wind turbine layout design and wind farm energy production estimation [26], [27]. After passing through upstream turbines, wind speed decreases and becomes turbulent, creating the wake effect phenomenon [28]. This phenomenon can occur within the same wind farm (internal) or between different wind farms (external). Operating turbines create two wake-affected zones called "near wake" and "far wake" [97], [30]. The near wake region extends 2-3 rotor diameters behind the turbine, where turbines directly disturb the wind. The far wake region lies beyond the near wake, extending 3-7 rotor diameters, typically affecting areas within large wind farms. For turbine layout optimization, the far wake region becomes more important than the near wake. This is especially critical when adding new turbines to upgrade or expand existing farms.

Several analytical wake models have been proposed, including the Jensen, Frandsen, Larsen, and Ishihara models [31]. The classical Jensen model [320], later refined by Katic [26], is among the most widely used due to its computational simplicity and acceptable accuracy for wind farm–scale modeling [33]–[36].

In the Jensen model, the wake region behind turbines is considered turbulent wind, while swirling wind flow effects are ignored. To determine wake effects, Jensen uses two parameters d_{normal} and R_w: when $d_{normal} < R_w$, downstream turbines are affected by wake; conversely, if $d_{normal} \geq R_w$, they are considered unaffected. However, this approach does not accurately reflect reality as it only considers two extreme states (completely affected or completely unaffected). To overcome this limitation, the Jensen-2D wake model was developed and proposed [37]–[39].

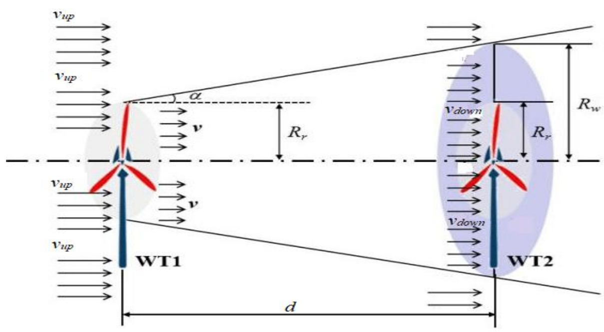

Fig. 1. Jensen's wake effect model [30].

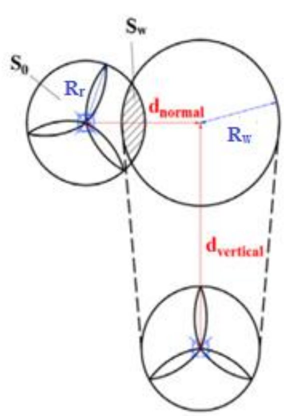

Fig.2. Jensen-2D wake effect model [37].

The Jensen-2D wake model is an advancement of the original Jensen formulation, incorporating the effect of partially overlapping wake zones on downstream turbines. In this model, the wake region is assumed to expand linearly with increasing downstream distance, forming a conical deficit region behind each turbine. The wake radius at a downstream distance d is given by:

$$R_w(d) = \kappa d + R_r \tag{1}$$

where, R_r is the rotor radius, κ is the wake decay constant, and d is the downstream distance.

The dimensionless one-dimensional constant κ determines the rate of wind expansion with distance and is defined as:

$$\kappa = \frac{0.5}{\ln \frac{H}{z_0}} \tag{2}$$

where, H is hub height and z_0 is the surface roughness constant, depending on terrain characteristics [38].

The velocity deficit at turbine j caused by turbine i is:

$$v_{def,j} = \frac{2a}{\left(1 + \frac{\kappa d_{ij}}{R_r}\right)^2} \tag{3}$$

where, a is the axial induction coefficient and is calculated by the following expression:

$$a = \frac{1}{2}\left(1 - \sqrt{1 - C_t}\right) \tag{4}$$

where, C_t is the turbine thrust coefficient [40] and v_{def} is the upstream wind velocity. When multiple turbines affect a single turbine, the total velocity deficit is calculated using:

$$v_{def}(j) = \sqrt{\sum_{j=1}^{N} v_{def}^2} \tag{5}$$

2.3 Wind Turbine Power Characteristics

Wind turbine power characteristics are determined by turbine manufacturers to help estimate wind power production in wind farm areas. Accurate modeling of turbine characteristics is crucial for predicting wind energy and supporting wind farm expansion [41], [42]. Many approaches to wind turbine characteristics have been introduced, including polynomial approximation [43]–[47]. In this study, a 9th-order polynomial model is applied as it was observed to be most suitable:

$$\begin{aligned} P(v) = {} & a_0 + a_1 v + a_2 v^2 + a_3 v^3 + a_4 v^4 + \\ & + a_5 v^5 + a_6 v^6 + a_7 v^7 + a_8 v^8 + a_9 v^9 \end{aligned} \tag{6}$$

This model accurately represents the nonlinear relationship between wind speed and power output in the region between cut-in and rated wind speeds. Along with the turbine power characteristic curve, the thrust coefficient (C_t) is very important for calculating wake effects in wind farms and wind farm performance [48], [49]

2.4 Energy Production Calculation

The annual energy output of each turbine accounts for wake-induced wind speed reductions by combining two components: the Weibull distribution, which describes the statistical frequency of wind speeds at the turbine site, and the power characteristic curve of the turbine, which maps wind speed to electrical output. For turbine i, the annual energy production is therefore computed as:

$$E_i = E_i^{v_{cut\_in} \to v_{rated}} + E_i^{v_{rated} \to v_{cut\_out}} \tag{7}$$

For $v_{cut\text{-}in} \le v < v_{rated}$:

$$E_i^{v_{cut\_in} \to v_{rated}} = T \cdot \sum_{h=1}^{h} f_i(\theta) \sum_{k=1}^{n_{div}} \int_{v_k}^{v_{k+1}} f(v) \frac{k_i(\theta)}{c_i(\theta)} \left(\frac{v}{c_i(\theta)} \right)^{k_i(\theta)-1} e^{-\left(\frac{v}{c_i(\theta)} \right)^{k_i(\theta)}} dv \tag{8}$$

For $v_{rated} \le v < v_{cut\text{-}out}$:

$$E_i^{v_{rated} \to v_{cut\_out}} = T \cdot \sum_{h=1}^{h} f_i(\theta) \sum_{k=1}^{m_{div}} \int_{v_k}^{v_{k+1}} P_{rated} \frac{k_i(\theta)}{c_i(\theta)} \left(\frac{v}{c_i(\theta)} \right)^{k_i(\theta)-1} e^{-\left(\frac{v}{c_i(\theta)} \right)^{k_i(\theta)}} dv \tag{9}$$

where, T = 8760 hours/year; h = 12 wind sectors; $f_h(\theta)$ = frequency of sector h; $f(v)$ = turbine power function (9th-order polynomial); $p(v,k,c)$ = Weibull probability density function; v = wind speed at turbine i in sector h considering wake effects:

Wind speed considering wind wake effect:

$$v = v_{up}\left(1 - v_{def,i}^{h}\right) \tag{10}$$

Therefore, the wind turbine characteristics are restated as follows:

$$f(v) = \begin{cases} 0, & v_i < v_{cut\,in}, v_i > v_{cut\,out} \\ P(v)\, in\, Eq.(6), & v_{cut\,in} \le v_i \le v_{cut\,out} \\ P_{rated}, & v_{rated} \le v_i \le v_{cut\,out} \end{cases} \tag{11}$$

2.5 Objective Function

Whether constructing a new wind farm or expanding an existing one, the spatial arrangement of turbines is among the most consequential engineering decisions, since it determines the degree to which wake losses reduce overall energy capture. Accordingly, the optimization problem is formulated to search for turbine layout configurations that maximize the aggregate annual energy production of the entire wind farm. The objective function takes the following form:

$$E_{total} = \sum_{i=1}^{N} E_i \tag{12}$$

$$Obj = \max\left(E_{total}\right) \tag{13}$$

2.6 Constraints

The optimization problem must satisfy several technical and operational constraints to ensure safe and efficient wind farm operation [94,119,124]:

Minimum distance constraint:

$$d_{ij} \ge d_{min} \tag{14}$$

where, d_{ij} is the distance between turbines i and j, d_{min} is the minimum safe distance $d_{min} = 3D_r$ to $5D_r$, and D_r is the rotor diameter.

Boundary constraints:

$$\begin{cases} X_{\min} \le x_i \le X_{\max} \\ Y_{\min} \le y_i \le Y_{\max} \end{cases}, \forall i \tag{15}$$

Wind speed operational limits:

$$v_{cut-in} \le v \le v_{cut-out} \tag{16}$$

3. 3. METHODOLOGY

3.1 Study Site and Data Collection

The study was conducted at a representative near-shore coastal site in the Mekong Delta. A multi-year measurement dataset (10–120 m) was used to characterize the vertical wind profile and long-term variability. The wind rose indicates three dominant wind sectors: easterly, northeasterly, and southwesterly, reflecting seasonal monsoon behavior typical of the region. Wind-speed statistics fitted with a two-parameter Weibull model show a mean value of 7.13 m/s, and turbulence intensity derived from 10-minute records remains within IEC Class III requirements.

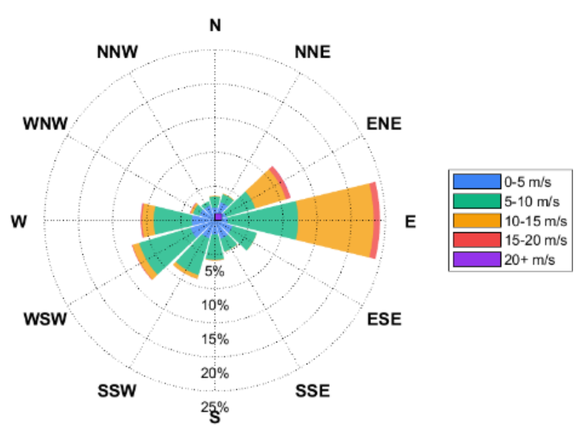

Fig. 3. Wind Rose.

The study site is located within the coastal region of southern Vietnam, characterized by stable monsoonal wind regimes and extremely flat terrain. The turbine-layout domain is defined in the UTM coordinate system (WGS84, Zone 48N), with Easting values from 523,500 m to 527,500 m and Northing values from 1,027,500 m to 1,031,000 m, corresponding to approximately 9.280°–9.311°N and 105.676°–105.713°E. Terrain elevation is nearly uniform, ranging from 0.5 m to 3.0 m above sea level, and surface roughness is consistently low (0.03–0.04 m) due to predominantly agricultural land cover with minimal obstructions. Land-availability constraints arise mainly from aquaculture areas, coastal protection buffers, and existing transport and utility corridors. These site-specific wind, terrain, and land-use characteristics provide a realistic and robust basis for numerical simulation, wake modeling, and turbine micro-siting for near-shore wind farm development in the Vietnamese coastal zone.

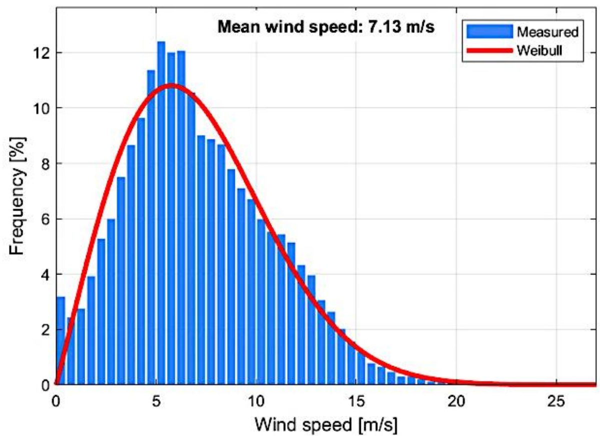

Fig.4. Wind speed distribution.

3.2 Turbine Models

The reference configuration is evaluated using three turbine ratings—3.0 MW, 3.45 MW, and 4.2 MW—as summarized in Table 1, which lists the turbine models considered for the wind farm analysis.

Table 1. Types of turbines proposed for wind farms [50]

Type of Turbine / Parameter	VESTAS		
	3.0 MW	**3.45 MW**	**4.2 MW**
Rated power (MW)	3.0	3.45	4.2
Rotor diameter (m)	90	112	150
Number of blades	3	3	3
Cut-in wind speed (m/s)	4.0	3.0	3.0
Rated wind speed (m/s)	15	13	10.1
Cut-off wind speed (m/s)	25	25	25
Hub height (m)	90	112	150
Number of turbine (N)	21	18	15

Figure 5 illustrates the polynomial-based performance model developed in this study, incorporating representative operational characteristics of modern wind turbines. The comparison indicates a strong agreement between the modeled and the actual turbine behavior. Specifically, Figure 3(a) shows the power curve of the VESTAS 3.0 MW unit, Figure 3(b) displays the characteristics of the VESTAS 3.45 MW turbine, and Figure 3(c) presents the performance profile of the VESTAS 4.2 MW turbine [50], [51].

This study examines a coastal wind farm in Vietnam. Site analysis indicates an average wind speed of 7.13 m/s and a wind power density of 380 W/m², as summarized in Table 2. Based on these site characteristics, the proposed optimization algorithms are employed to determine the optimal turbine layout that maximizes energy output and capacity factor. The results provide a basis for recommending the turbine type most suitable for the local wind conditions.

Table 2. Input parameters

Input parameters	
Roughness (Z_0)	0.038
Wind velocity in free flow (V_0)	7.13 m/s
Wind density	380 W/m^2
Wind farm area	4000 m x 3500 m

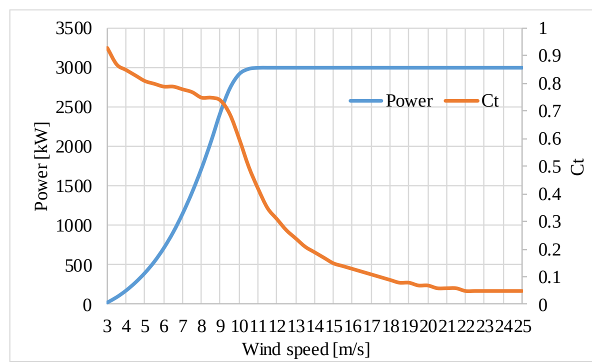

(a) VESTAS-3.0MW turbine.

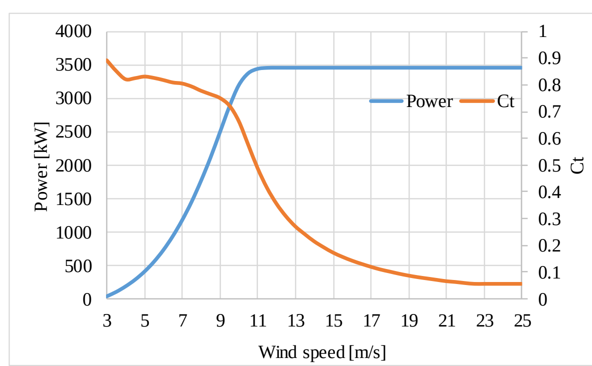

(b) VESTAS-3.45MW turbine.

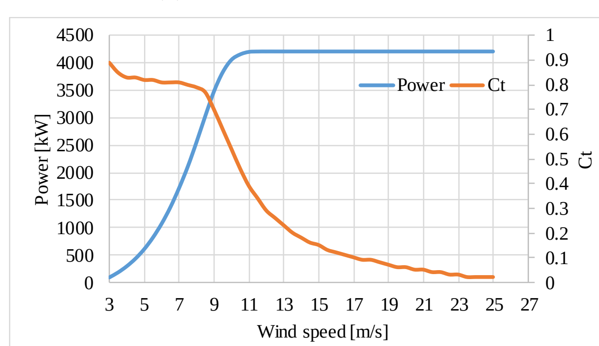

(c) VESTAS-4.2MW turbine

Fig. 5. Turbine characteristics.

3.3 SOS Optimization Framework

3.3.1 Algorithm Overview

Originally developed by Cheng and Prayogo [16], [52]–[55], the Symbiotic Organisms Search (SOS) is a population-based metaheuristic algorithm whose search strategy is inspired by the co-evolutionary dynamics found in natural ecosystems. The algorithm models three categories of interspecies relationships: mutualism, where a cooperative interaction yields fitness gains for both parties; commensalism, where only one organism benefits while its counterpart experiences no change; and parasitism, where one organism exploits another to its own advantage. Starting from a randomly generated initial population, the algorithm evolves candidate solutions across successive generations through these three phases, applying a greedy selection mechanism that preserves superior solutions. Iteration continues until the specified stopping criterion is reached.

3.3.2 SOS Phases for Wind Turbine Optimization

Initialization:

Each solution X_i represents a turbine layout configuration. For new construction: $X_i = [(x_1, y_1),(x_2, y_2), \ldots, (x_n, y_n)]$. For upgrade/expansion: X_i includes both existing and new turbine positions. The initial population is randomly generated within boundary constraints:

$$X_i = lb + rand(0,1) \times (ub - lb) \tag{17}$$

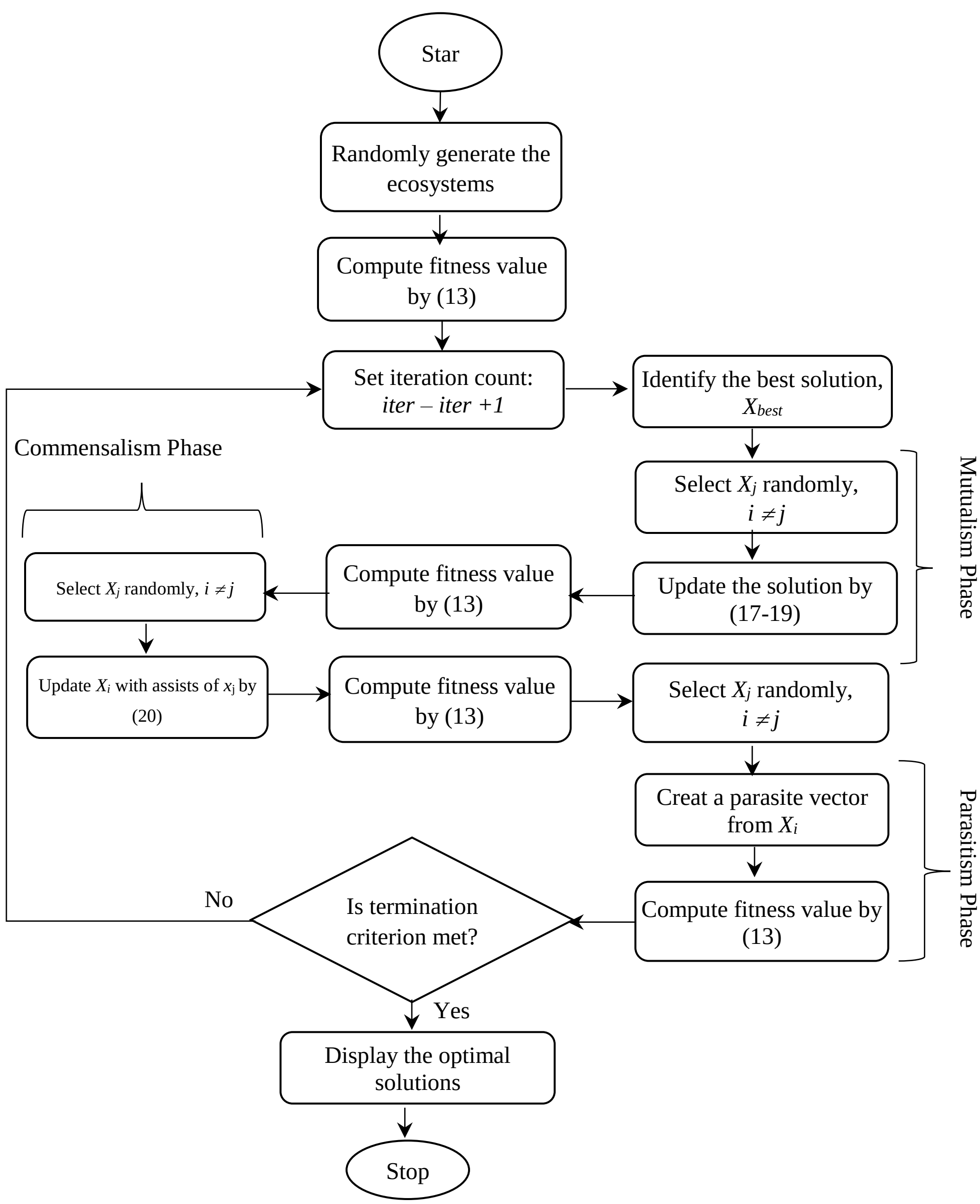

Fig. 6. Flowchart of the SOS algorithm [55].

Phase 1: Mutualism Phase

In this phase, two randomly selected layout configurations X_i and X_j interact with each other to enhance their chances of obtaining the best layout. New configurations for X_i and X_j are generated according to:

$$X_{inew} = X_i + rand(0,1)*(X_{best} - MV*BF1) \quad (18)$$

$$X_{jnew} = X_j + rand(0,1)*(X_{best} - MV*BF2) \quad (19)$$

where, $MV = (X_i + X_j)/2$, BF_1, $BF_2 \in \{1, 2\}$ are benefit factors ranging from 1-2, and X_{best} is the current best solution. The term (X_{best} - MV) reflects efforts to increase the rate of achieving the best objective function value.

Phase 2: Commensalism Phase

As in the mutualism stage, two randomly selected configurations, (X_i) and (X_j), from the ecosystem are chosen to interact with each other.In this interaction, configuration X_i benefits while X_j is neither benefited nor affected. The new configuration of X_i is modeled as:

$$X_{inew} = X_i + rand(-1,1)*\left(X_{best} - X_j\right) \quad (20)$$

The benefit in this case is provided by (X_{best} - X_j) where configuration X_j provides maximum benefit to X_i.

Phase 3: Parasitism Phase

In this phase, a configuration X_i is randomly selected from the ecosystem to create a parasite vector – i.e., a configuration mutated from X_i. Duplicate or invalid elements in the vector are replaced with random values to maintain population diversity. The parasite vector then competes with another configuration X_j; if it has a higher objective value (energy production), it replaces X_j, otherwise it is eliminated.

3.3.3 Algorithm Parameters

A population size of 45 was selected in accordance with common recommendations for metaheuristic optimization, where values between 20 and 50 are typically considered effective. The SOS algorithm is relatively simple to parameterize, requiring only the specification of the number of organisms and the total iterations, which enhances its stability and ease of implementation. The upper limit of 1000 iterations was adopted to provide an appropriate compromise between computational effort and solution convergence. In addition, the benefit factors were randomly assigned values of 1 or 2 to emulate either partial or complete mutualistic interactions, thereby maintaining the stochastic balance between exploration and exploitation as suggested in previous studies [54].

3.4 Application Procedure

The SOS is applied to optimize wind turbine layout through the following systematic procedure:

Step 1: Set problem parameters - Define wind data (speed, direction, Weibull distribution), terrain data (elevation, surface roughness), turbine specifications (power curve, thrust coefficient), existing turbine positions (for upgrade/expansion scenarios), and technical constraints.

Step 2: Initialize SOS parameters - Set population size (Organisms = 45), maximum iterations (*MaxIter* = 800), benefit factors (BF_1, $BF_2 \in \{1,2\}$), and search space boundaries (*lb*, *ub*).

Step 3: Run SOS algorithm - Execute iterative optimization through mutualism, commensalism, and parasitism phases, updating solutions based on fitness evaluation.

Step 4: Evaluate solutions – Wake-affected wind speeds are computed using the Jensen–2D model (Section 2.2), followed by AEP calculation for each layout.

Step 5: Check and enforce constraints - Verify minimum distance requirements, boundary compliance, and collision avoidance with existing turbines; apply repair mechanisms for violations.

Step 6: Output results - Return optimal turbine positions, total AEP, capacity factor, and convergence history

The algorithm continues running until it reaches the specified maximum number of iterations or meets the convergence conditions, ultimately producing an optimized turbine arrangement that maximizes energy output while satisfying all technical and spatial requirements.

All wake modeling equations and aerodynamic assumptions strictly follow the formulations presented in Section 2.

4. RESULTS AND DISCUSSION

This section presents an integrated evaluation of turbine–wind compatibility, energy-yield performance, and spatial optimization. The discussion synthesizes findings from capacity factor (CF) analysis, annual energy production (AEP), algorithmic convergence, and wake–spacing interactions to assess the suitability of the three commercial turbines for the medium-wind coastal site.

4.1 Turbine Selection Proposal Using Wind Probability and Power Curves

This study presents a preliminary assessment of suitable wind turbine models by combining the site's wind-speed probability distribution with the operational characteristics of three commercial turbines currently deployed in Vietnam (3.0 MW, 3.45 MW, and 4.2 MW) [53]. The local wind regime is dominated by speeds of 7–8 m/s, with peak occurrence probabilities of 10–11%, while the effective operating range of 6–10 m/s accounts for the majority of annual hours. These features classify the site as a medium-wind location, where the match between the turbine's rated wind speed and the most frequent wind speeds plays a decisive role in maximizing annual energy production (Figure 7).

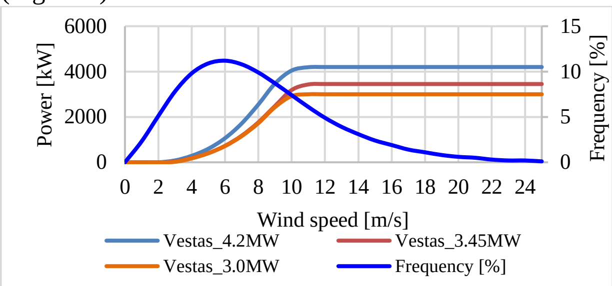

Fig. 7. Wind frequency distribution and turbine power curves.

The wind-speed probability distribution was overlaid with the power curves of the three turbine models. All candidates are compatible with the dominant 7–13 m/s range; however, their operational responses differ. The 3.0 MW turbine, with a 90-m rotor and 15 m/s rated speed, maintains efficient output across 7–15 m/s and aligns well with the high-frequency 8–12 m/s band. The 3.45 MW turbine (112 m, 13 m/s rated) performs strongly in the 8–11 m/s range but requires larger spacing, reducing feasible turbine count. The 4.2 MW turbine (150 m, 10.1 m/s rated) reaches full capacity earliest but suffers from extensive wake zones, allowing only 15 turbines to be deployed within the 4 km × 3.5 km site.

Quantitative integration of the power curves with the Weibull distribution indicates that the 3.0 MW turbine achieves the highest weighted power coefficient in the 7–11 m/s interval (0.387), outperforming the 3.45 MW (0.361) and 4.2 MW (0.342) models. Its smaller swept area also enables higher turbine density and greater installed capacity per unit land area. Overall, preliminary analysis identifies the 3.0 MW turbine as the most favorable choice, combining optimal power-curve compatibility, layout flexibility, and superior energy-capture potential.

Figure 8 presents the convergence characteristics of the SOS, GA, PSO methods when applied to the wind turbine layout optimization problem. The objective function reflects wake-induced power losses, and the average best-so-far fitness value is recorded over 800 iterations to evaluate the stability and search efficiency of each algorithm. The convergence profiles provide a quantitative basis for assessing the relative performance of the three methods under identical experimental conditions.

Figure 8 illustrates the convergence characteristics of SOS, GA, and PSO for the 3 MW, 3.45 MW, and 4.2 MW turbine cases. Across all configurations, SOS consistently achieves the lowest objective values and converges faster than the other two algorithms, demonstrating strong exploitation ability and stable search performance. GA shows moderate convergence, with an initial rapid decrease followed by stagnation, while PSO converges more slowly and settles at higher objective values. The similarity in convergence patterns for all three turbine capacities confirms the robustness of SOS and its superior balance between exploration and exploitation in solving the turbine layout optimization problem.

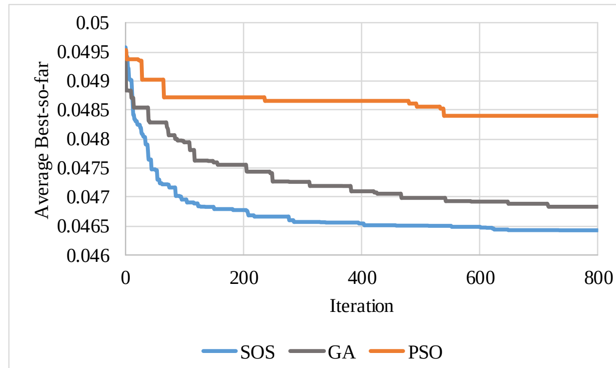

(a) 3.0 MW Turbine.

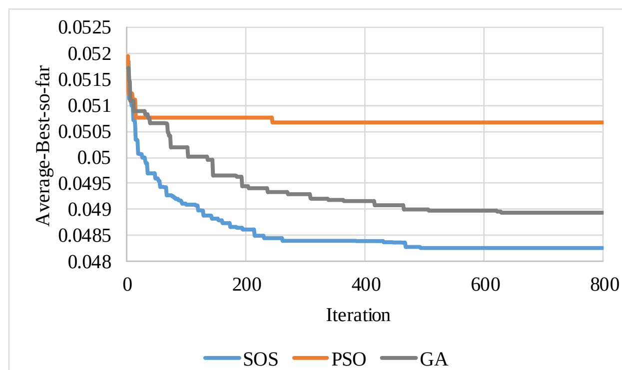

(b) 3.45 MW Turbine.

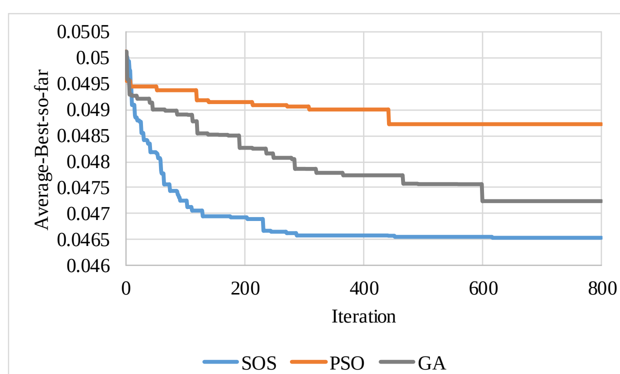

(c) 4.2 MW Turbine.

Fig. 8. Convergence curves of the SOS, GA, and PSO algorithms.

Table 3. Convergence Speed Comparison (3.0 MW Turbine)

Algorithm	90% Optimal	95% Optimal	99% Optimal

SOS	180	320	580
GA	280	520	750
PSO	420	680	800

To further quantify the convergence differences, Table 1 reports the number of iterations required for each algorithm to reach 90%, 95%, and 99% of the optimal objective value in the 3.0 MW turbine case. These metrics offer a clearer assessment of computational efficiency and reveal how rapidly each method approaches near-optimal performance.

As shown in Table 3, SOS demonstrates consistently faster convergence across all optimization thresholds. SOS reaches 90% of the optimal solution in 180 iterations—36% faster than GA (280 iterations) and 57% faster than PSO (420 iterations). This performance advantage becomes even more pronounced at higher convergence levels: SOS requires 38% fewer iterations than GA and 27% fewer than PSO to achieve 95% optimality. At the 99% threshold, SOS converges in 580 iterations compared to 750 for GA, while PSO fails to reach this level within the 800-iteration limit. These results quantitatively confirm the superior convergence efficiency of SOS, which stems from its balanced exploration-exploitation mechanism through mutualism, commensalism, and parasitism phases that enable more effective navigation of the complex solution landscape.

4.2. Capacity Factor Analysis of Candidate Turbines

Selecting the optimal turbine model for a given site requires evaluating how effectively each candidate harnesses the prevailing wind conditions. To this end, the capacity factor (CF) was computed for all three turbine models using the empirically derived wind speed probability distribution at the site. As a dimensionless ratio of actual annual energy yield to the turbine's theoretical maximum output, the CF provides a direct measure of each turbine's compatibility with the local wind regime. The comparative results, summarized in Table 4, reveal a clear and consistent performance hierarchy among the three candidates.

Table 4. Capacity factor comparison with solution quality metrics

Turbine	Algorithm	Best CF (%)	Mean CF (%)	Std Dev (%)	Wake Loss (%)
3.0 MW	**SOS**	34.37	34.12	0.08	8.2
	GA	34.08	33.88	0.23	9.7
	PSO	33.05	32.68	0.52	11.8
3.45 MW	**SOS**	33.61	33.38	0.09	10.7
	GA	33.12	32.87	0.27	11.9
	PSO	31.98	31.64	0.57	13.4
4.2 MW	**SOS**	34.03	33.94	0.09	11.3
	GA	33.68	33.52	0.25	12.6
	PSO	32.69	32.37	0.53	14.1

The enhanced capacity factor analysis presented in Table 3 reveals not only the mean performance but also the consistency and reliability of each optimization algorithm across 30 independent runs. SOS achieves the highest mean CF (34.12%) for the 3.0 MW turbine with remarkably low standard deviation (0.08%), demonstrating exceptional solution quality and consistency. In comparison, GA produces a mean CF of 33.88% with higher variability (σ = 0.23%), while PSO exhibits the lowest mean CF (32.68%) and the highest variability (σ = 0.52%). This pattern holds consistently across all three turbine configurations, with SOS maintaining standard deviations of 0.08-0.09% compared to 0.23-0.27% for GA and 0.52-0.57% for PSO. The superior consistency of SOS reflects its robust search mechanism that reliably identifies near-optimal layouts without being trapped in local optima, a critical advantage for commercial wind farm development where predictable performance is essential for financing and operational planning.

To strengthen the comparative assessment, each algorithm was executed in 30 independent runs, and the results were analyzed using the Wilcoxon signed-rank test [57]. The SOS algorithm exhibits statistically significant superiority over GA ($p < 0.01$) and PSO ($p < 0.001$). Combined with the updated multi-seed convergence curves, these findings demonstrate that SOS consistently delivers higher AEP and exhibits markedly greater stability and robustness in the optimization process.

4.3. Annual Energy Production (AEP) Estimation

AEP was calculated for each turbine model by integrating the turbine power curves with the site-specific wind-speed probability distribution. This approach provides a quantitative measure of the total annual energy yield and enables direct comparison of turbine performance under identical meteorological conditions. The AEP estimation accounts for turbine availability, air-density corrections, and typical wake losses, ensuring that the resulting values reflect realistic operational expectations.

Table 5 indicates clear performance differentiation among the algorithms, with SOS consistently delivering the highest annual energy production (AEP) across 30 optimization runs. AEP was computed using turbine power curves, the site-specific Weibull distribution, Jensen–2D wake modeling (α = 0.075), 97% availability, coastal air-density correction, and 3% electrical losses. For the 3.0 MW configuration, SOS achieves the highest mean AEP (188.29 GWh/year) with exceptional stability (CV = 0.22%), outperforming GA by 1.23 GWh/year and PSO by 7.86 GWh/year—differences that translate to meaningful revenue gains under typical coastal PPA conditions.

provide a consolidated view of how technical performance translates into economic feasibility at the wind farm scale.

Table 5. Annual energy production with solution quality metrics

Turbine	Algorithm	Best AEP (GWh/yr)	Mean AEP (GWh/yr)	Std Dev (GWh)	CV (%)
3.0 MW	**SOS**	188.76	188.29	0.42	0.22
	GA	187.84	187.06	1.28	0.68
	PSO	182.14	180.43	2.87	1.59
3.45 MW	**SOS**	182.03	181.58	0.51	0.28
	GA	180.76	179.92	1.45	0.81
	PSO	175.38	173.62	3.12	1.80
4.2 MW	**SOS**	187.85	187.28	0.48	0.26
	GA	186.14	185.23	1.37	0.74
	PSO	180.52	178.76	2.95	1.65

The 3.0 MW layout provides the best overall performance due to its favorable balance between capacity (63 MW), compatibility with the dominant 7–11 m/s wind regime, and low wake losses (8.2%). Although 4.2 MW turbines yield competitive AEP, their reduced unit count and higher wake losses limit overall effectiveness. The 3.45 MW configuration performs lowest because of less optimal power-curve matching and higher wake interference.

Solution-quality metrics further highlight algorithmic reliability. SOS maintains the lowest variability (CV = 0.22–0.28%), whereas GA and PSO exhibit 3–6 times higher variability, indicating greater sensitivity to local optima. For the 3.0 MW scenario, PSO's standard deviation is 583% higher than SOS, underscoring its reduced consistency. This stability gives SOS a clear advantage in project planning, where dependable production forecasts are essential for financing and PPA negotiations.

Together, the highest mean AEP, lowest variability, and superior wake management confirm that the SOS-optimized 3.0 MW configuration is the most technically robust and financially attractive option for medium-wind coastal sites.

To evaluate the economic performance of the three turbine configurations, the Levelized Cost of Energy (LCOE) was computed using the AEP results obtained from the SOS-optimized layouts. Table 5 summarizes the comparative LCOE values alongside the corresponding installed capacities and annual energy production. These metrics

Table 6. LCOE Comparison of Turbines

Parameter	Vestas 3.0 MW	Vestas 3.45 MW	Vestas 4.2 MW
Rated power (MW/turbine)	3	3.45	4.2
Total installed capacity (MW)	63	62.1	63
AEP (GWh/year)	188.29	181.58	187.28
LCOE (USD/MWh)	41.8	42.7	42.1
NPV (MUSD)	89.3	83.6	87.8
Payback period (years)	14.4	13.7	12.7

To link the technical optimization results with project-level economics, a simple payback analysis was performed using the current Vietnamese onshore wind feed-in tariff of 1,587.12 VND/kWh [58] (approximately 60 USD/MWh at late-2025 exchange rates). Annual revenues were computed as the product of the feed-in tariff and AEP, and annual net cash flow was obtained by subtracting the corresponding OPEX from this revenue. The resulting payback periods for the SOS-optimized layouts are 14.4, 13.7, and 12.7 years for the 3.0, 3.45, and 4.2 MW configurations, respectively. Although the 4.2 MW layout benefits from the shortest payback due to its higher per-turbine output, the 3.0 MW configuration remains the most attractive long-term investment option because it combines the lowest LCOE (41.8 USD/MWh), the highest NPV (89.3 MUSD), and the largest annual energy yield among the evaluated designs.

To evaluate algorithmic robustness under varying wind conditions—a critical consideration for coastal wind farms subject to monsoon-driven seasonal variability—sensitivity analysis was conducted by testing each algorithm under three distinct wind regime scenarios. The baseline scenario represents medium-wind conditions (7-9 m/s mean speed), corresponding to the site's measured wind characteristics. Low-wind (5-7 m/s) and high-wind (9-11 m/s) scenarios simulate periods of reduced or enhanced wind activity, respectively. For each scenario, wind speed distributions were adjusted while maintaining the directional frequency pattern, and 30 independent optimization runs were performed. Performance stability was quantified as the percentage of baseline AEP maintained under each condition. Table 7 presents the robustness analysis results for the 3.0 MW turbine configuration, which demonstrated the highest overall performance.

The robustness analysis in Table 7 shows that SOS maintains highly stable performance under wind variations aligned with the site's dominant east, east-northeast, and southwest directions. When wind speeds decrease, SOS preserves 96.2% of its baseline output—higher than GA (91.3%) and PSO (88.4%)—indicating lower sensitivity to temporary reductions in the easterly flow. Under stronger winds, SOS again performs best, retaining 97.8% stability compared with 93.7% for GA and 90.2% for PSO, demonstrating effective wake mitigation across both ENE and SSW wind corridors.

Table 7. Robustness analysis under variable wind regimes (3.0 MW turbine)

Algorithm	Low-Wind (5-7 m/s)	Medium-Wind (7-9 m/s)	High-Wind (9-11 m/s)
SOS	96.2%	100%	97.8%
GA	91.3%	100%	93.7%
PSO	88.4%	100%	90.2%

This robustness stems from SOS's adaptive search dynamics, which avoid over-fitting to a single wind scenario and instead produce layouts that perform consistently across multiple prevailing directions. Such stability is particularly valuable for coastal Vietnamese wind farms, where seasonal shifts alternate between ENE and SSW wind regimes. Overall, the superior stability metrics indicate that SOS-optimized layouts deliver more reliable energy output and reduce uncertainty in long-term production forecasts.

4.4. Layout Optimization and Site Integration

Following the turbine performance assessment, a layout optimization analysis was conducted to evaluate how each turbine model integrates within the site's spatial constraints and prevailing wind characteristics. The optimization process aims to maximize energy yield while minimizing wake losses, which are known to significantly reduce downstream turbine output in medium-wind environments.

The optimized layouts reveal distinct performance differences among the three algorithms. The SOS configuration places 21 turbines with effective 3.5–4.0D spacing and staggered alignment with the 90° and 240° wind directions, yielding the lowest wake losses (8.2%) and the highest array efficiency (91.8%), as illustrated in Figures 9–11. The GA layout, while maintaining the same turbine count, features tighter 3.0–3.2D spacing and insufficient lateral offsets, increasing wake losses to 9.7% and reducing array efficiency to 90.3%. The PSO layout performs worst, with turbine clustering, marginal 2.8–3.0D spacing, misalignment with dominant wind sectors, and underutilization of site area, leading to 11.8% average wake losses and array efficiency of only 88.2%. These spatial patterns directly correspond to the AEP hierarchy observed in Section 4.3.

The results presented in Sections 4.1–4.4 collectively identify the 3.0 MW turbine, optimized using the SOS algorithm, as the most suitable configuration for medium-wind coastal sites. Power-curve analysis (Section 4.1) shows that this turbine aligns most effectively with the site's 7–11 m/s wind regime, yielding the highest weighted power coefficient. Capacity factor evaluation (Section 4.2) further confirms its advantage, with a CF of 34.12%, exceeding both the 4.2 MW and 3.45 MW alternatives. Annual energy production analysis (Section 4.3) demonstrates that the 3.0 MW layout achieves the highest AEP (188.29 GWh/year), resulting in the lowest LCOE and strongest project economics. Layout optimization results (Section 4.4) reinforce these conclusions, as the SOS algorithm consistently outperforms GA and PSO by ensuring lower wake losses, more effective turbine spacing, and superior spatial utilization.

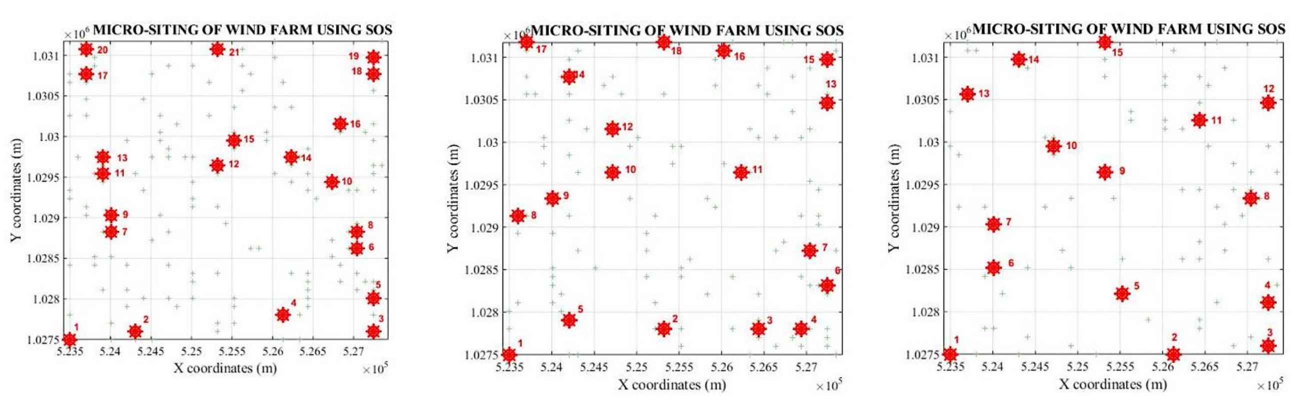

(a) Layout for the Vestas 3.0 MW turbine

(b) Layout for the Vestas 3.45 MW turbine

(c) Layout for the Vestas 4.2 MW turbine

Fig. 9. Optimal wind turbine layouts obtained using the SOS algorithm.

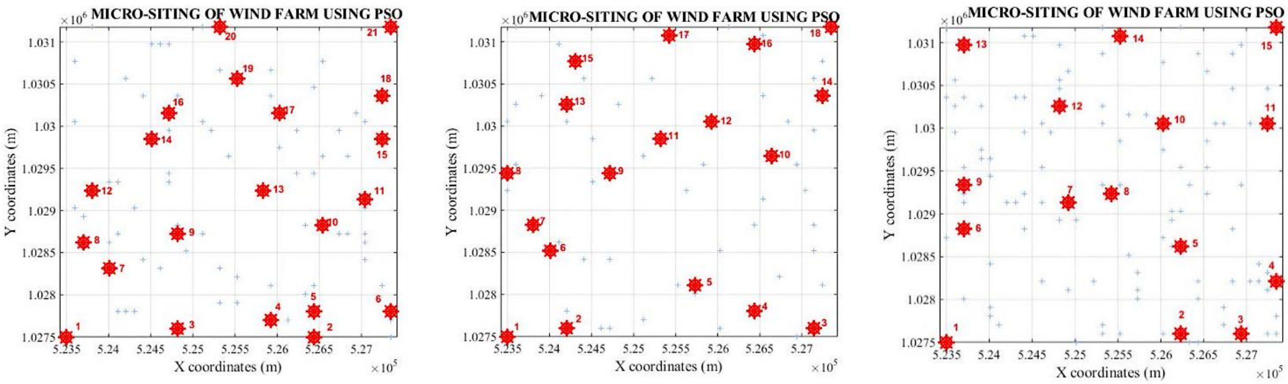

(a) Layout for the Vestas 3.0 MW turbine (b) Layout for the Vestas 3.45 MW turbine (c) Layout for the Vestas 4.2 MW turbine

Fig.10. Optimal wind turbine layouts obtained using the PSO algorithm.

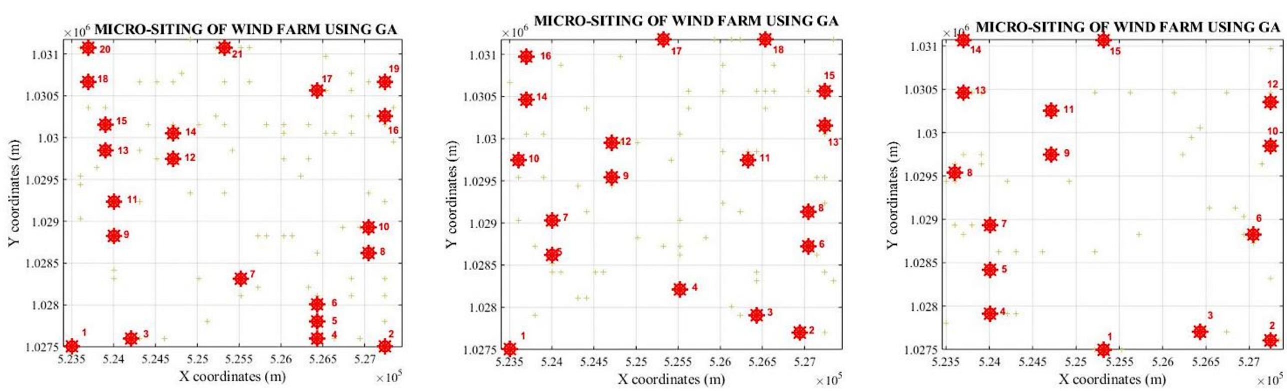

(a) Layout for the Vestas 3.0 MW turbine (b) Layout for the Vestas 3.45 MW turbine (c) Layout for the Vestas 4.2 MW turbine

Fig.11. Optimal wind turbine layouts obtained using the GA algorithm.

Taken together, these convergent findings provide a rigorous and coherent technical basis for turbine selection, farm-layout design, and optimization strategy in coastal wind developments. The integrated framework and demonstrated performance advantages offer practical guidance for future projects in Vietnam and can be readily applied to similar medium-wind coastal environments across Southeast Asia.

The results of this study offer several practical implications for wind farm development in Vietnam's coastal regions. First, the optimal 3.0 MW turbine configuration demonstrates the highest energy density, which is particularly important for narrow coastal areas with limited available land. Second, the smaller rotor diameter contributes to reduced wake expansion and improved layout flexibility, a critical factor in monsoon-dominated wind regimes where directional wake amplification can significantly affect performance. Third, the lower LCOE associated with the optimized configuration enhances project bankability and aligns with Vietnam's national renewable energy targets under PDP-VIII [59]. These findings provide actionable guidance for developers and policymakers regarding turbine selection, land-use planning, and investment strategies for future coastal wind projects.

4.5. Sensitivity Analysis

To evaluate framework robustness and transferability, sensitivity analysis was conducted across two critical environmental dimensions: seasonal monsoon variability and terrain roughness. These factors represent primary sources of uncertainty in coastal wind farm performance, particularly in monsoon-influenced regions where wind patterns and land-use conditions vary significantly. The SOS-optimized 3.0 MW configuration serves as the baseline reference for all sensitivity assessments.

4.5.1. Seasonal Monsoon Variability

Coastal wind resources in Vietnam and throughout Southeast Asia are strongly influenced by the Asian monsoon system, creating distinct seasonal regimes. The northeast monsoon (November-April) is characterized by dominant east (E) and east-northeast (ENE) winds with higher speeds and greater consistency, while the southwest monsoon (May-October) brings west-southwest (WSW) winds of moderate intensity. Wind speed distributions were

reconstructed for three periods based on multi-year site measurements. The seasonal performance analysis for the SOS-optimized 3.0 MW turbine configuration is presented in Table 8.

Table 8. Seasonal monsoon performance analysis

Monsoon Period	Dominant Wind Direction	Mean Speed (m/s)	Seasonal AEP (GWh)	% of Annual AEP	Performance Stability (%)
Northeast Monsoon (Nov-Apr)	E, ENE	8.2	112.4	59.7	106.8
Southwest Monsoon (May-Oct)	WSW, SW	6.3	65.1	34.6	97.9
Transition Periods	Variable	5.1	10.8	5.7	94.3
Annual Weighted Average	—	**7.13**	**188.3**	**100.0**	**100.0**

The analysis reveals that the northeast monsoon contributes disproportionately to annual production, generating 59.7% of total AEP despite comprising only 50% of the year. The dominant east (E) and east-northeast (ENE) winds during this period, with mean speeds of 8.2 m/s, achieve 106.8% performance stability, reflecting effective turbine alignment and wake management under high-wind conditions from these directions. The southwest monsoon maintains robust production (34.6% of annual AEP) with 97.9% stability despite west-southwest (WSW) winds at reduced mean speeds (6.3 m/s), demonstrating balanced performance across both primary wind directions. Transition periods contribute 5.7% with 94.3% stability under variable wind directions. The relatively modest seasonal variation (±6.8%) is substantially smaller than inter-algorithm differences (±15-20% between SOS and PSO observed in Section 4.3), confirming that optimization algorithm selection has greater impact than seasonal variability. These findings enable accurate monthly revenue forecasting and validate framework transferability to other monsoon-influenced coastal sites throughout Southeast Asia.

4.5.2. Terrain Roughness Sensitivity

Surface roughness length (z_0) directly influences vertical wind profiles and wake decay characteristics. Performance was evaluated across five representative z_0 values spanning realistic coastal terrain conditions, from smooth tidal flats (z_0 = 0.01 m) to suburban environments (z_0 = 0.10 m). The wake decay coefficient (α) was recalculated for each roughness condition using Equation (2), maintaining the SOS-optimized turbine positions of the 3.0 MW configuration from baseline (z_0 = 0.038 m). Table 7 presents the comprehensive terrain sensitivity results.

Table 9. Terrain roughness sensitivity analysis

Terrain Type	z_0 (m)	Wake Decay α	AEP (GWh/yr)	Wake Loss (%)	Relative Performance (%)
Very Smooth	0.01	0.063	196.2	6.8	104.2
Smooth	0.03	0.071	190.7	7.5	101.3
Agricultural (Baseline)	0.038	0.075	188.3	8.2	100.0
Light Agriculture	0.05	0.080	184.5	9.1	98.0
Suburban	0.10	0.095	177.4	11.2	94.2

The analysis reveals systematic relationships between terrain roughness and performance. AEP increases by 4.2% when roughness decreases from baseline (z_0 = 0.038 m) to very smooth conditions (z_0 = 0.01 m), primarily through faster wake recovery (α = 0.063) that reduces wake losses from 8.2% to 6.8%. Conversely, AEP decreases by 5.8% under suburban conditions (z_0 = 0.10 m) due to slower wake recovery (α = 0.095) that increases wake losses to 11.2%. The intermediate scenarios (z_0 = 0.03 and 0.05 m) show modest deviations of +1.3% and -2.0%, indicating robust performance across typical coastal agricultural conditions. The pronounced sensitivity to extreme roughness values underscores the importance of accurate terrain characterization and suggests optimal site selection should prioritize locations with z_0 < 0.05 m. The demonstrated performance range of 94.2-104.2% across realistic terrain scenarios validates the SOS framework's robustness and applicability to diverse coastal environments throughout Southeast Asia.

The combined sensitivity analyses demonstrate that the SOS-optimized framework delivers stable, predictable performance across environmental conditions likely in coastal wind farm development. The modest variations under seasonal changes (±6.8%) and terrain roughness variations (±4.2%) are substantially smaller than inter-algorithm performance differences (±15-20%), reinforcing the critical importance of optimization algorithm selection. These findings support framework transferability to commercial wind projects in monsoon-influenced coastal regions worldwide and provide quantitative evidence for robust performance under realistic operational variability.

5. LIMITATIONS AND FUTURE WORK

Although the proposed SOS-based micro-siting framework demonstrates strong performance for the examined coastal wind farm in Vietnam, several methodological limitations should be acknowledged. First, the optimization process employs a fixed discretized grid, which restricts spatial flexibility and may prevent the identification of truly optimal layouts in irregular or highly constrained terrain. Future research will explore adaptive grid refinement and continuous spatial-search techniques to improve the resolution and robustness of turbine positioning. Second, the wake modeling approach relies on the Jensen and Jensen–2D formulations, both of which assume linear wake expansion, steady inflow conditions, and simplified turbulence–wake interactions. These assumptions may limit accuracy under complex atmospheric stability regimes or heterogeneous flow conditions. Incorporating higher-fidelity wake models—such as CFD-based or LES-based simulations—represents an important direction for enhancing predictive capability. Third, the current framework does not explicitly integrate spatially varying terrain elevation, surface roughness, or dynamic land-use constraints. Future work will consider the incorporation of digital elevation models, roughness maps, and geospatial exclusion layers to increase applicability to real-world planning scenarios. Finally, extending the SOS optimization methodology to offshore applications—where wake recovery characteristics, boundary-layer dynamics, and installation constraints differ substantially—offers a promising avenue for further advancement.

6. CONCLUSION

This study developed an integrated framework for wind turbine selection and layout optimization tailored to medium-wind coastal environments. By combining site-specific wind probability distributions, detailed power-curve evaluation, wake-loss modeling, and SOS algorithm, the framework provides a systematic approach for maximizing annual energy production while minimizing wake interactions. Among the three turbine models examined, the 3.0 MW turbine achieved the highest weighted power coefficient, the largest capacity factor, and the lowest wake losses, enabling the deployment of 21 units and producing the maximum annual energy output of 188.29 GWh/year. This configuration also yielded the lowest levelized cost of energy and the highest net present value, confirming its technical and economic superiority.

Algorithmic comparisons further demonstrated that SOS consistently outperformed GA and PSO across all performance metrics, increasing AEP by up to 1.2% over GA and 4.6% over PSO. These gains result from SOS's balanced search mechanism, which effectively navigates the multimodal layout optimization landscape and delivers robust, low-variance solutions suitable for real-world wind farm planning.

The findings have broader implications for Vietnam's renewable energy development. The optimized 3.0 MW configuration supports the deployment goals outlined in PDP-VIII by enhancing energy density, reducing costs, and improving feasibility in land-constrained coastal regions. Its strong performance under monsoon-driven wind variability aligns with national objectives for energy security and the commitment to achieving net-zero emissions by 2050.

Overall, the study identifies the SOS-optimized 3.0 MW configuration as the most technically sound and economically feasible option for medium-wind coastal sites, and the proposed framework remains applicable to similar environments across Southeast Asia. Future research will extend this approach by incorporating long-term wind variability, grid-integration constraints, and multi-objective optimization to explicitly evaluate trade-offs among AEP, wake losses, and land-use limitations, thereby further improving its robustness for utility-scale wind farm development.

ACKNOWLEDGMENT

We acknowledge Ho Chi Minh City University of Technology, VNU-HCM for supporting this study.

NOMENCLATURE

Symbol	Description
AEP	Annual Energy Production (MWh/year)
CF	Capacity Factor (%)
CV	Coefficient of Variation
V_{def}	Wake deficit
D_r	Rotor diameter (m)
H	Hub height (m)
NPV	Net Present Value
PDP	Power Development Plan
PPA	Power Purchase Agreement
$P(v)$	Power output at wind speed v (kW)
P_{rated}	Rated power of turbine (MW)
v	Wind speed (m/s)
$f(v)$	Wind-speed probability distribution
Ct	Thrust coefficient
θ	Wind direction (°)

REFERENCES

[1] International Energy Agency (IEA). 2023. Net Zero Roadmap: A Global Pathway to Keep the 1.5°C Goal in Reach. Paris: IEA.
[2] IPCC. 2023. AR6 Synthesis Report: Climate Change 2023. Geneva: IPCC.
[3] Olauson, J. 2022. Trends in wind turbine technology over the

past four decades. Energy Conversion and Management 269: 116082.
[4] International Renewable Energy Agency (IRENA). 2023. Renewable Power Generation Costs in 2022. Abu Dhabi: IRENA.
[5] Global Wind Energy Council (GWEC). 2024. Global Wind Report 2024. Brussels: GWEC.
[6] World Bank and ESMAP. 2021. Vietnam Wind Atlas 2021. Washington, DC: World Bank.
[7] Ministry of Industry and Trade (MOIT). 2023. Vietnam National Power Development Plan VIII. Hanoi: MOIT.
[8] Shapiro, C.; Meyers, J.; and Meneveau, C. 2022. Wind farm layout optimization considering wake effects. Renewable Energy 190: 695-709.
[9] Wang, S. and Wang, S. 2025. Impacts of wind turbine characteristics on wake turbulence. Energy Storage and Conversion 3: 1956.
[10] Nguyen, K. 2022. Wind energy in Vietnam: Resource assessment, development status and future implications. Energy Policy 35: 1405-1413.
[11] Linh, D.; Dung, T.; and An, T.D. 2025. Long-term wind energy potential analysis in Vietnam's central highlands using the innovative trend analysis method. Asian Journal of Water, Environment and Pollution 23: 025370289.
[12] Kumar, M.; Sharma, A.; Sharma, N.; Sharma, F.B.; and Bhadu, M. 2024. Wind farm layout optimization problem using nature-inspired algorithms. Journal of Electrical and Computer Engineering 2024: 9406519.
[13] El Jaadi, M.; Haidi, T.; and Belfqih, A. 2024. Advancements in wind farm layout optimization: a comprehensive review of artificial intelligence approaches. TELKOMNIKA (Telecommunication Computing Electronics and Control) 22: 763-772.
[14] Masoudi, S.M. and Baneshi, M. 2022. Layout optimization of a wind farm considering grids of various resolutions, wake effect, and realistic wind speed and wind direction data: A techno-economic assessment. Energy, Elsevier 244(PB).
[15] Croonenbroeck, C. and Hennecke, D. 2020. A comparison of optimizers in a unified standard for optimization on wind farm layout optimization. Energy 216: 119244.
[16] Gharehchopogh, F.S.; Shayanfar, H.; and Gholizadeh, H. 2020. A comprehensive survey on symbiotic organisms search algorithms. Artificial Intelligence Review 53: 2265-2312.
[17] Saremi, S.; Mirjalili, S.; and Lewis, A. 2017. Grasshopper optimisation algorithm: Theory and application. Advances in Engineering Software 105: 30-47.
[18] Hossam, F.; Ibrahim, A.; Majdi, M.; and Asghar, H.A. 2020. Salp swarm algorithm: Theory, literature review, and application in extreme learning machines. Studies in Computational Intelligence 2020: 185-199.
[19] Tran, H.; Sentchev, A.; Thai, D.T.; Herrmann, M.; Ouillon, S.; and Nguyen, K.C. 2025. Surface circulation characterization along the middle southern coastal region of Vietnam from high-frequency radar and numerical modeling. Ocean Science 21: 1-8.
[20] Mai, V.K.; Nguyen, B.T.; Tran, V.L.; Vu, V.T.; Du, D.T.; Pham, T.H.T.; and Hole, L.R. 2025. Evaluation of wind energy potential over offshore areas in Vietnam. Vietnam Journal of Marine Science and Technology 25 (3): 269-284.
[21] Dykes, K.; Meadows, R.; Felker, F.F.; Graf, P.A.; Hand, M.; Lunacek, M.; Michalakes, J.; Moriarty, P.J.; Musial, W.; and Veers, P.S. 2011. Applications of systems engineering to the research, design, and development of wind energy systems. Technical Report NREL/TP-5000-52921. Golden, CO: National Renewable Energy Laboratory.
[22] Abdulrahman, M. and Wood, D. 2017. Investigating the power-COE trade-off for wind farm layout optimization considering commercial turbine selection and hub height variation. Renewable Energy 102: 267-278.
[23] Bouchekara, H.R.E.H.; Sha'aban, Y.A.; Shahriar, M.S.; Ramli, M.A.M.; and Mas'ud, A.A. 2023. Wind farm layout optimisation considering commercial wind turbines using parallel reference points, radial space division and reference vector guided EA-based approach. Energy Reports 9: 4919-4940.
[24] Burton, T.; Jenkins, N.; Sharpe, D.; and Bossanyi, E. 2021. Wind Energy Handbook. 3rd ed. Chichester: Wiley.
[25] Carta, M.; Mentado, M.; and Ramirez, J. 2009. A review of wind speed probability distributions used in wind energy analysis: Case studies in the Canary Islands. Renewable and Sustainable Energy Reviews 13 (5): 933-955.
[26] Katic, J.; Hojstrup, J.; and Jensen, N. 1986. A simple model for cluster efficiency. Proceedings of the European Wind Energy Association Conference. Rome, Italy, 7-11 October 1986. pp. 407-410.
[27] Crespo, A. and Hernandez, J.A. 1996. Turbulence characteristics in wind-turbine wakes. Journal of Wind Engineering and Industrial Aerodynamics 61: 71-85.
[28] Vermeer, L.; Sorensen, J.N.; and Crespo, A. 2003. Wind turbine wake aerodynamics. Progress in Aerospace Sciences 39: 467-510.
[29] Doubrawa, P.; Montornes, A.; Barthelmie, R.; Pryor, S.; Giroux, G.; and Casso, P. 2017. Effect of wind turbine wakes on the performance of a real case WRF-LES simulation. Journal of Physics: Conference Series 854: 012010.
[30] Bastankhah, M. and Porte-Agel, F. 2014. A new analytical model for wind-turbine wakes. Renewable Energy 70: 116-123.
[31] Sorensen, J.N. 2011. Aerodynamic aspects of wind energy conversion. Annual Review of Fluid Mechanics 43: 427-448.
[32] Jensen, N.O. 1983. A note on wind generator interaction. Report No. Riso-M-2411. Roskilde: Riso National Laboratory.
[33] Frandsen, S. 1992. On the wind speed reduction in the center of large clusters of wind turbines. Journal of Wind Engineering and Industrial Aerodynamics 39: 251-265.
[34] Larsen, G.C. 2009. A simple stationary semi-analytic wake model. Report No. Riso-R-1356. Roskilde: Riso National Laboratory.
[35] Qian, G.W. and Ishihara, T. 2018. A new analytical wake model for yawed wind turbines. Energies 11 (3): 665.
[36] Ma, K.; Zhang, H.; Gao, X.; Wang, X.; Nian, H.; and Fan, W. 2024. Research on evaluation method of wind farm wake energy efficiency loss based on SCADA data analysis. Sustainability 16 (5): 1813.
[37] Tian, L.; Zhu, W.J.; Shen, W.Z.; Zhao, N.; and Shen, Z. 2015. Development and validation of a new two-dimensional wake model for wind turbine wakes. Journal of Wind Engineering and Industrial Aerodynamics 137: 90-99.
[38] Lu, P.; Wang, Y.; Zhou, Y.; Ge, M.; and Li, R. 2025. Large-eddy simulation of wind farm wake behavior and power

efficiency: Effects of atmospheric stratification and staggered configurations. Boundary-Layer Meteorology 249: 123075.

[39] Gao, X.; Yang, H.; and Lu, L. 2016. Optimization of wind turbine layout position in a wind farm using a newly developed two-dimensional wake model. Applied Energy 174: 192-200.

[40] Vahidi, D. and Porte-Agel, F. 2025. Influence of thrust coefficient on the wake of a wind turbine: A numerical and analytical study. Renewable Energy 240: 122194.

[41] Lydia, M.; Kumar, S.S.; Selvakumar, A.I.; and Kumar, G.E.P. 2014. A comprehensive review on wind turbine power curve modeling techniques. Renewable and Sustainable Energy Reviews 30: 452-460.

[42] Sohoni, V.; Gupta, S.; and Nema, R. 2016. A critical review on wind turbine power curve modelling techniques and their applications in wind-based energy systems. Journal of Energy 2016: 8519785.

[43] Bilendo, F.; Meyer, A.; Badihi, H.; Lu, N.; Cambron, P.; and Jiang, B. 2023. Applications and modeling techniques of wind turbine power curve for wind farms - A review. Energies 16 (1): 180.

[44] Carrillo, C.; Montano, A.F.O.; Cidras, J.; and Diaz-Dorado, E. 2013. Review of power curve modelling for wind turbines. Renewable and Sustainable Energy Reviews 21: 572-581.

[45] Tautz-Weinert, J. and Watson, S. 2017. Using SCADA data for wind turbine performance monitoring. IET Renewable Power Generation 11 (4): 403-413.

[46] Ouyang, T.; Kusiak, A.; and He, Y. 2017. Modeling wind-turbine power curve: A data partitioning and mining approach. Renewable Energy 102: 1-8.

[47] Al-Quraan, A.; Al-Masri, H.; Al-Mahmodi, M.; and Radaideh, A. 2021. Power curve modelling of wind turbines - A comparison study. IET Renewable Power Generation 16: 2916-2930.

[48] Martinez-Tossas, L.A.; Annoni, J.; Fleming, P.A.; and Churchfield, M.J. 2022. Numerical investigation of wind turbine wakes under high thrust coefficient. Wind Energy 25 (4): 605-617.

[49] Bourhis, M.; Messmer, T.; Holling, M.; and Buxton, O.R.H. 2025. Impact of free-stream turbulence and thrust coefficient on wind turbine-generated wakes. Journal of Fluid Mechanics 1023: A3.

[50] Wind-Turbine-Models.com. 2023. List of Vestas Turbine Models. [Online]. Retrieved September 1, 2025 from https://en.wind-turbine-models.com/turbines?manufacturer=17&view=table

[51] Vestas Wind Systems A/S. 2023. Material Use in Vestas Turbines. Sustainability Brochure. [Online]. Retrieved September 1, 2025 from https://www.vestas.com/content/dam/vestas-com/global/en/sustainability/environment/2023_04_Material-Use-Brochure_Vestas.pdf

[52] Cheng, M.Y. and Prayogo, D. 2014. Symbiotic organisms search: A new metaheuristic optimization algorithm. Computers and Structures 139: 98-112.

[53] Guha, D.; Roy, P.; and Banerjee, S. 2018. Symbiotic organism search algorithm applied to load frequency control of multi-area power system. Energy Systems 9: 439-468.

[54] Nguyen, K.D.; Tran, T.T.; and Vo, D.N. 2025. Optimal turbine placement in wind power plants using search algorithms. Journal of Electrical Engineering and Technology 20: 2107-2119.

[55] Nguyen, K.D.; Tran, T.T.; Dao, T.; Tran, N.A.; Nguyen, P.D.D.; and Vo, D.N. 2025. Strategic turbine addition in existing wind farms: A symbiotic organisms search algorithm approach. Proceedings of the 2025 International Symposium on Electrical and Electronics Engineering (ISEE) - Power and Energy Systems. Ho Chi Minh City, Vietnam, October 2025. pp. 208-213.

[56] Gupta, M.; Gautam, A.; Yadav, H.; Gupta, P.; Sarkar, J.; and Sarkar, A. 2025. Assessment of wind energy potential and turbine selection for sustainable energy generation in India. Energy Sources, Part A: Recovery, Utilization, and Environmental Effects 47 (1): 120-134.

[57] Derrac, J.; Garcia, S.; Molina, D.; and Herrera, F. 2011. A practical tutorial on the use of nonparametric statistical tests as a methodology for comparing evolutionary and swarm intelligence algorithms. Swarm and Evolutionary Computation 11: 3-18.

[58] Ministry of Industry and Trade of Vietnam. 2022. Circular No. 15/2022/TT-BCT: Regulations on Methodology for Developing Electricity Generation Price Framework for Transitional Solar and Wind Power Plants. Hanoi, Vietnam.

[59] Government of Vietnam. 2023. National Power Development Plan VIII (PDP VIII) for the Period 2021-2030 with a Vision to 2050. Decision No. 500/QD-TTg. Hanoi, Vietnam.